

# Vibrational dynamics and boson peak in a supercooled polydisperse liquid

Sneha Elizabeth Abraham and Biman Bagchi\*

*Solid State and Structural Chemistry Unit, Indian Institute of Science, Bangalore 560 012, India*

(Dated: February 24, 2009)

Vibrational density of states (VDOS) in a supercooled polydisperse liquid is computed by diagonalizing the Hessian matrix evaluated at the potential energy minima for systems with different values of polydispersity. An increase of polydispersity leads to an increase in relative population of the localized high-frequency modes. At low frequencies, the density of states show an excess compared to the Debye squared-frequency law, which has been identified with the boson peak. The height of the boson peak increases with polydispersity. The values of the participation ratio as well as the level spacing statistics demonstrate that the modes comprising the boson peak are largely delocalized. Interestingly, the intensity of the boson peak shows a rather narrow sensitivity to changes in temperature and is seen to persist even at high temperatures. Study of the difference spectrum at two different polydispersity reveals that the increase in the height of boson peak is due to a population shift from modes with frequencies above the maximum in the VDOS to that below the maximum, indicating an increase in the fraction of the unstable modes in the system. The latter is further supported by the facilitation of the observed dynamics by polydispersity. Since the strength of the liquid increases with polydispersity, the present result provides an evidence that the intensity of boson peak correlates positively with the strength of the liquid, as observed earlier in many experimental systems.

PACS numbers: 63.50.Lm, 64.70.pm, 82.70.Dd

## I. INTRODUCTION

A glass behaves mechanically like a solid but structurally like a liquid with relaxation times varying from a few minutes to several centuries. The elasticity of a solid is described in terms of phonons, which are quantized vibrational excitations. Propagating acoustic phonon-like excitations have been observed in glasses and glass-forming liquids down to wavelengths comparable to interparticle distance [1]. However, their description is rendered difficult since glasses lack the translational invariance of crystalline solids. A ubiquitous feature in the physics of glasses is the anomalous behavior of the low-frequency part of the vibration spectrum and the corresponding thermal properties [2]. While the origin of the linear low-temperature specific heat is commonly attributed to the existence of double-well potentials or two-level systems, there is a considerable debate about the so-called *boson peak* [3, 4]. This peak shows up in the vibrational density of states (VDOS),  $g(\nu)$  as an excess contribution, compared to the usual Debye behavior [ $g(\nu) \propto \nu^2$ ]. It is called boson peak because the temperature dependence of its intensity scales roughly with the Bose-Einstein distribution. In addition to the presence of boson peak (BP) (or excess density of states) at low frequencies, one also observes a high-frequency exponential tail [5] in the reduced density of states spectrum.

The interpretation of the boson peak has been a challenge to experimentalists and theoreticians and is a sub-

ject of controversial discussions. While some authors attribute it to local/quasi-local vibrations [3, 6, 7, 8], some others attribute it to collective motions [5, 9]. A universal mechanism of the BP formation in glasses was proposed based on the concept of interacting quasi-local oscillators [8]. Boson peak has also been explained in terms of the affine-non-affine crossover at a certain mesoscopic length scale [10]. It has also been interpreted as the signature of a phase transition in the space of the stationary points of the energy, from a minima-dominated phase (phonons) at low energy to a saddle dominated phase (without phonons) [11]. The boson peak has also been linked to those motions giving rise to the two-level-like excitations seen at still lower temperatures [12]. Recently evidence was presented from numerical studies suggestive of the equality of the boson peak frequency to the Ioffe-Regel limit for transverse phonons above which transverse phonons do not propagate, and the boson peak was attributed to transverse vibrational modes associated with defective soft structures in the disordered state [13].

Optical heterodyne-detected optical Kerr effect data on supercooled acetylsalicylic acid and dibutylphthalate display highly damped oscillations with a period of a few pico seconds as the temperature is reduced to and below the Mode Coupling Theory temperature,  $T_{MCT}$  [14]. The authors interpret this as the time domain signature of the boson peak and explain that the increased translational-rotational coupling is responsible for the boson peak as  $T < T_{MCT}$ . The main experimental tools used for the investigation of VDOS and boson peak in glasses are Raman scattering and the quasi-elastic neutron scattering (QENS). Recently, single-molecule spectroscopic studies have also emerged as a potential tool to study the boson peak in glasses [7]. The main difficulty

---

\*email: bbagchi@sscu.iisc.ernet.in

here is the conflicting interpretations regarding the origin of the boson peak. For instance, nuclear inelastic scattering studies of ferrocene probe molecules in toluene, ethylbenzene, dibutylphthalate and glycerol glasses show that a significant part of the modes constituting the boson peak is of collective character [5]. However, from the single molecule spectroscopic studies of many single tetra-tert-butylterrylene molecules embedded to amorphous polyisobutylene the authors conclude that the low-energy vibrational excitations have a local character [7].

The theoretical as well as experimental studies are done on systems/samples in the glassy state. However, since the the phonon-like excitations also persist at elevated temperatures in the supercooled liquid regime [1], one can study the vibrational dynamics of supercooled liquids via molecular dynamics simulations. Various groups have studied the vibrational dynamics of supercooled liquids [15, 16, 17, 18], where the focus has been on the characteristics of the high-frequency or low-frequency vibrational modes. The main emphasis of these studies have been on the collective/local nature of the vibrational modes.

In this study we investigate the vibrational dynamics and boson peak in a polydisperse Lennard-Jones liquid. Polydisperse liquid is one of the simplest model systems that exhibit glass transition and can be conveniently studied via both experiments [19, 20] and computer simulations as the size distribution of particles prevents crystallization [21, 22, 23]. The rest of the paper is organized as follows. In section II we describe the model and computational details. In section III we present our results and give detailed discussions on the same. We give our concluding remarks in section IV.

## II. COMPUTATIONAL DETAILS

Micro canonical ensemble molecular dynamics (MD) simulations are carried out in three dimensions on a system of Lennard-Jones (LJ) particles of mean diameter  $\bar{\sigma}$  with polydispersity in both size and mass. The polydispersity in size is introduced by random sampling from the Gaussian distribution of particle diameters  $\sigma$ ,

$$P(\sigma) = \frac{1}{\sqrt{2\pi}\delta} \exp\left[-\frac{1}{2}\left(\frac{\sigma - \bar{\sigma}}{\delta}\right)^2\right] \quad (1)$$

The standard deviation  $\delta$  of the distribution divided by its mean  $\bar{\sigma}$  gives a dimensionless parameter, the polydispersity index,  $S$

$$S = \frac{\delta}{\bar{\sigma}} \quad (2)$$

The mass  $m_i$  of particle  $i$  is scaled by its diameter,

$$m_i = \bar{m} \left(\frac{\sigma_i}{\bar{\sigma}}\right)^3 \quad (3)$$

We have chosen  $\bar{m} = 1.0$ . The simulations are carried out at different values of the polydispersity index,  $S$  but at

fixed volume fraction,  $\phi = 0.54$ . Three different system sizes were chosen,  $N = 256, 500$  and  $864$ . The results are found to be qualitatively the same for the three different system sizes studied.

The interactions between the particles are given by the shifted-force LJ potential

$$U_{ij} = 4\epsilon_{ij} \left[ \left(\frac{\sigma_{ij}}{r_{ij}}\right)^{12} - \left(\frac{\sigma_{ij}}{r_{ij}}\right)^6 \right] \quad (4)$$

where  $i$  and  $j$  represent any two particles and

$$\sigma_{ij} = \left(\frac{\sigma_i + \sigma_j}{2}\right) \quad (5)$$

The LJ interaction parameter  $\epsilon_{ij}$  is assumed to be the same for all particle pairs and set equal to unity. The particles are enclosed in a cubic box and periodic boundary conditions are used. The cutoff radius  $r_c$  is chosen to be  $2.5\bar{\sigma}$ . The time step used for integrating the equations of motion is 0.001. All quantities in this study are given in reduced units (length in units of  $\sigma$ , temperature in units of  $\frac{\epsilon}{k_B}$  and time in units of  $\tau = \left(\frac{m\sigma^2}{\epsilon}\right)^{\frac{1}{2}}$ ).

The vibrational density of states is obtained from the Normal Mode Analysis by solving the secular equation,

$$|\mathbf{F} - \nu^2 \mathbf{I}| = 0 \quad (6)$$

Here  $F$  is the mass-weighted potential energy matrix (also known as the Hessian matrix),

$$F_{ij} = \frac{V_{ij}}{\sqrt{m_i m_j}} \quad (7)$$

Equation 6 can be solved to yield a set of eigen values (the square of the vibrational frequencies,  $\nu^2$ ) and corresponding eigen vectors (normal mode displacement vectors),  $\mathbf{e}_i$ . From the equilibrium liquid configurations generated by the MD simulations, one constructs the potential energy minima or the inherent structure via conjugate gradient minimization. From the potential energy minima, one generates the Hessian matrix, the diagonalization of which would yield the eigen values and the eigen vectors. The normal modes thus obtained are called the *quenched normal modes* (QNM).

Instantaneous normal modes (INM) can be obtained by diagonalizing the Hessian constructed for the equilibrium liquid configurations. Since the instantaneous liquid configuration is not necessarily a potential energy minimum, one gets both unstable modes (negative eigen values or imaginary frequencies) and stable modes (positive eigen values).

## III. RESULTS AND DISCUSSION

### A. Polydispersity Effects on Vibrational Density of States

The configuration-averaged vibrational density of states,  $g(\nu)$  for the quenched normal modes is shown in

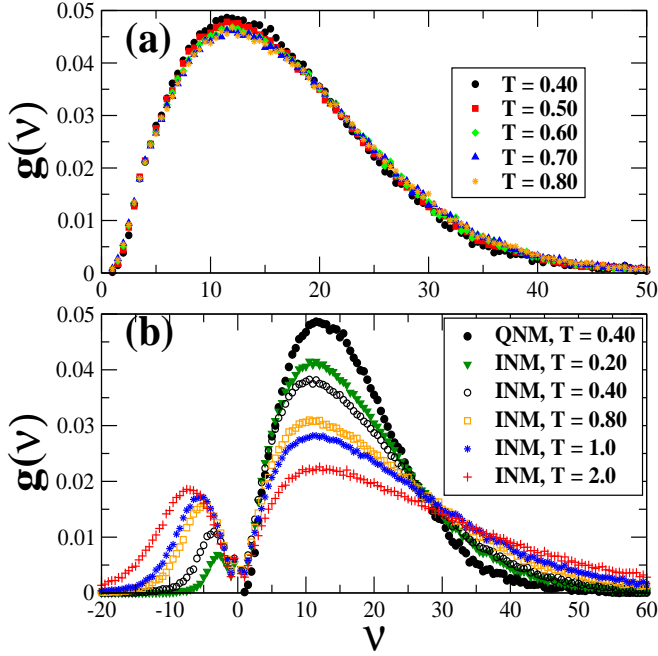


FIG. 1: (a) Quenched normal mode spectra at different values of  $T$ . The data is for  $S = 0.20$  and system size  $N = 256$ . (b) Instantaneous normal mode spectra for different values of  $T$ . As  $T$  decreases the INM spectra approaches closer to the quenched spectrum (dark circles).

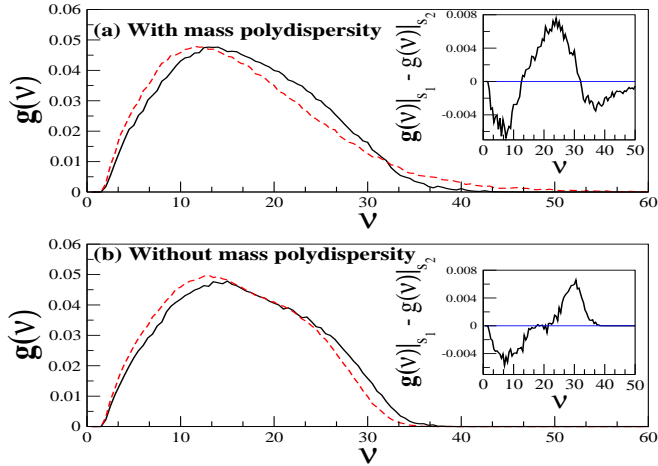


FIG. 2: (a)  $g(\nu)$  for  $S = 0.10$  and  $S = 0.20$  systems and their difference (inset) (b) Same as (a) but for  $S = 0.10$  and  $S = 0.20$  systems without mass polydispersity. Data shown for a system of  $N = 256$  particles.

FIGURE 1(a) for  $S = 0.20$  at different values of temperature. The width of the bin chosen to build the histogram is 0.50. The VDOS is rather featureless as has been observed by Rahman et al [24] for single-component Lennard-Jones system. From FIGURE 1(a), we see that the quenched normal density of states are only weakly

sensitive to the temperature of the parent liquid. The rather narrow sensitivity of the quenched normal mode spectra to temperature is to be contrasted with the instantaneous normal mode spectra obtained from equilibrium liquid configurations (See FIGURE 1(b)). The imaginary modes in the INM spectra are displayed on the negative side of the frequency axis. Both the stable (positive frequencies) and unstable (imaginary frequencies) modes of the INM spectrum show a pronounced change with temperature. As the temperature decreases, the fraction of the unstable modes decreases whereas that of the stable modes increases. At low temperature ( $T \leq 0.40$ ), the fraction of the unstable modes is considerably less, indicating that most of the particles are located near the potential energy minima most of the time.

Polydispersity has three noticeable effects on the vibrational density of states. Firstly, as polydispersity increases, the number of low frequency modes increases whereas the number of high frequency modes decreases (See FIGURE 2). Because of these compensating changes occurring in the high and low frequency regions, one observes a crossover in the density of states between  $S = 0.10$  and  $S = 0.20$  systems. For the data shown in FIGURE 2, this happens at a frequency  $\nu \sim 12.0$  for systems with mass polydispersity and  $\nu \sim 16.0$  for systems without mass polydispersity.

Secondly, when mass polydispersity is present, there is a second crossover point in the density of states between  $S = 0.10$  and  $S = 0.20$  systems at a frequency,  $\nu \sim 32$  (FIGURE 2(a)). For frequencies higher than this value, there is an excess of high-frequency modes that increases with  $S$ . This is best seen in the semi-log plot of  $g(\nu)$  in FIGURE 3. The plot clearly shows that as polydispersity increases there is a substantial increase in the number of high frequency modes. The polydispersity-dependence of the INM spectra is shown in FIGURE 4. The  $S = 0.20$  system has relatively higher number of high frequency modes for both the stable and unstable branches. In FIGURE 5, we show the semi-log plot of VDOS for different  $S$  but without mass polydispersity (i.e. all masses set equal to unity,  $m_i = 1.0$ ). As we can see from the figure, the number of high-frequency modes decreases with  $S$  for systems having no mass polydispersity. Thus the excess high frequency modes (whose fraction increases with increase in polydispersity) is due to the mass polydispersity effect rather than size polydispersity effect. (Below we show that the high frequency vibrations are all localized.) Thirdly, the vibrational density of states spectrum becomes narrower with polydispersity. In FIGURE 6 we plot the full width at half maximum (FWHM) of  $g(\nu)$  for  $S = 0.10$  and  $S = 0.20$  as function of  $T$ . The FWHM decreases sharply with  $S$  but shows only a weak increase with temperature.

The localization properties of the normal modes can be quantified via the participation ratio (PR) which is a measure of the number of particles participating in a given vibrational mode. The participation ratio of mode

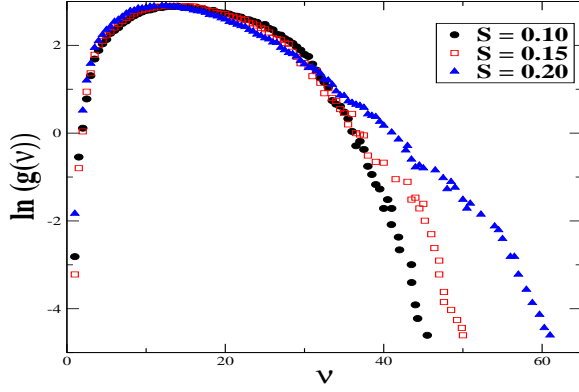


FIG. 3: Semilog plot of density of states. The data is for  $T = 0.50$ . The high frequency modes are localized (See Fig 7)

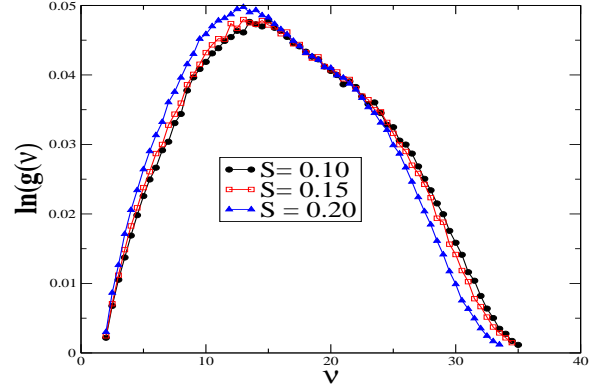


FIG. 5: Semilog plot of density of states for different  $S$  without mass polydispersity. The data is for  $T = 0.50$ .

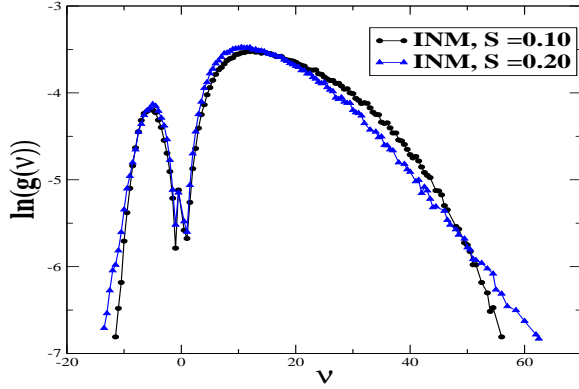


FIG. 4: Instantaneous normal mode spectrum for  $S = 0.10$  and  $S = 0.20$  systems at  $T = 0.80$ .

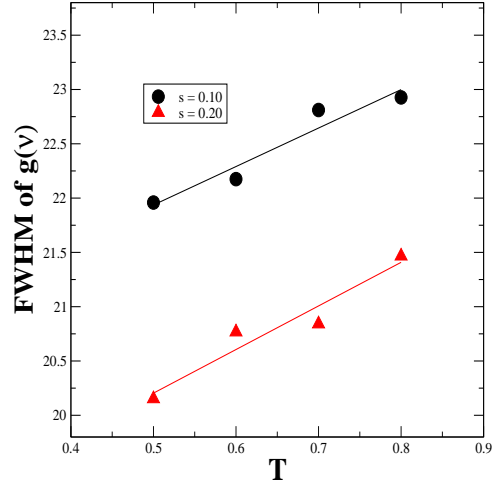


FIG. 6: Full width at half maximum, FWHM for  $S = 0.10$  and  $S = 0.20$  as a function of  $T$ .

$i$  is defined as

$$PR_i = [N \sum_{\alpha=1}^{3N} (e_i^\alpha \cdot e_i^\alpha)^2]^{-1} \quad (8)$$

The participation ratio is of the order of  $\frac{1}{N}$  for localized modes and is of the order of 1 for extended modes. In FIGURE 7, the participation ratio of the modes is plotted. The averaging is done over modes corresponding to eigenvalues in a histogram bin of width 0.50. As one can see from the plot, for  $\nu > 30.0$ , the participation ratio is very low, indicating that the high-frequency modes are all localized. Therefore the high-frequency tail of the normal mode spectrum can be attributed to the localized vibrations. In a crystalline solid, localized vibrations occur due to the presence of very light impurity atoms or interstitial atoms (that cause large lattice strains). It has been shown that when the mass of the impurity atom in a crystal is smaller than that of the other particles, the vibrations do not propagate through the system but gets localized around the impurity particle [25].

In the frequency range  $3.0 \leq \nu \leq 35$ , one finds delo-

calized modes as implied by the high values of PR. The participation ratio of the modes decreases with polydispersity for modes of all frequencies(See FIGURE 7) implying that the number of particles participating in a mode of given frequency decreases with  $S$ . Thus the vibrations become more localized with  $S$ . This means that as size disparity among the particles increases, the system cannot sustain propagating modes. It is interesting to note here that the large size disparity among the particles also leads to the suppression of growth of dynamic heterogeneity with polydispersity in supercooled liquids(See [23]). Dynamic heterogeneity in supercooled liquids in its simplest sense means clusters of fast-moving particles that move together for a certain amount of time before they get decorrelated. When size disparity is large, the particle motion gets decorrelated much faster and hence the formation of *dynamic* clusters is suppressed at higher polydispersity. In the inherent structure formalism developed by Stillinger and Weber [26, 27], the configuration

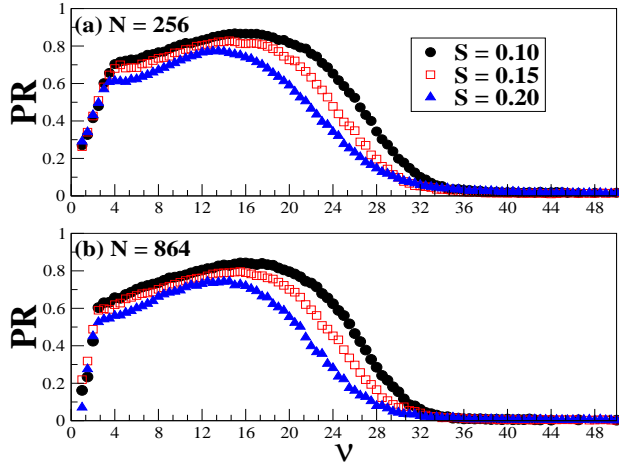


FIG. 7: Participation ratio (PR) of the modes for system sizes, (a)  $N = 256$  and (b)  $N = 864$ . PR gives the number of particles participating in a given mode. The data is shown for different  $S$  at  $T = 0.50$ . The plot shows that a  $S$  increases, the number of particles participating in a given mode decreases for all frequencies.

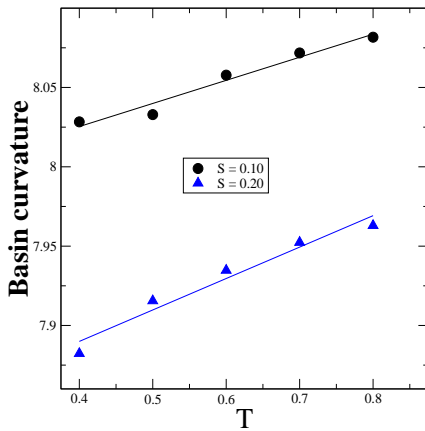


FIG. 8: Basin curvature as a function of temperature for  $S = 0.10$  and  $S = 0.20$  systems.

space of the liquid is divided into basins of local potential energy minima (or inherent structures). In the harmonic approximation, which is valid at sufficiently low temperatures, each basin is treated as a harmonic well. In FIGURE. 8 we plot the quantity  $N^{-1} \sum_{k=1}^{3N-3} \log(h\nu_k)$  as a function of  $T$  for  $S = 0.10$  and  $S = 0.20$  systems. This quantity is an indicator of the average curvature of the basins [28]. Since it is a sum of logarithms it is very sensitive to the tail of the spectrum. From the plot we see that the average curvature of the basins increases with  $T$  but decreases sharply with polydispersity. In other words, increasing polydispersity leads to a *flattening* of the basins which would in turn facilitate inter-basin transitions and thus enhances the mobility of the system. The latter has been termed the lubrication effect [22].

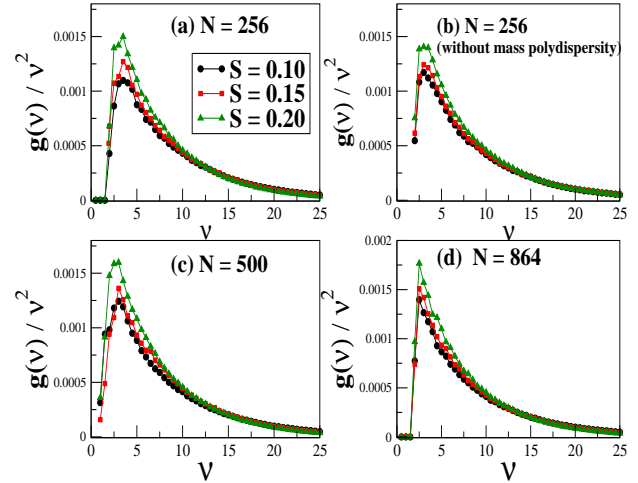


FIG. 9: Excess density of states (Boson Peak),  $\frac{g(\nu)}{\nu^2}$  versus  $\nu$ . Data shown for different  $S$  with the temperature of the parent liquid at  $T = 0.50$  and for system sizes, (a)  $N = 256$  (b)  $N = 256$  but without mass polydispersity (c)  $N = 500$  and (d)  $N = 864$ .

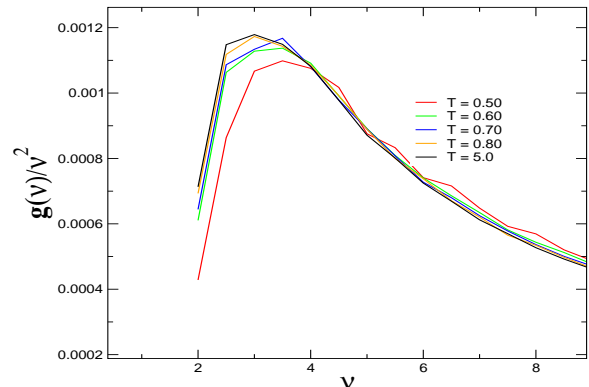


FIG. 10: Temperature dependence of the Boson Peak. The data is shown for  $S = 0.10$  for different temperatures of the parent liquid.

## B. Boson Peak

We plot the reduced density of states,  $g(\nu)/\nu^2$  in FIGURE 9 for three values of  $S$ , namely  $S = 0.10, 0.15$  and  $0.20$ . All the three systems exhibit the boson peak feature viz. excess density of states as compared to the prediction of the Debye model ( $g(\nu) \sim \nu^2$ ). As seen from the figure, the intensity of the boson peak,  $I_{BP}$  increases with  $S$  for all the three system sizes studied. However, *there is no noticeable change in the frequency of the Boson peak,  $\nu_{BP}$* . The boson peak feature is seen even when we switch off the mass polydispersity (See FIGURE 9 (b)) implying that the size polydispersity effect alone can give rise to the observed features. Furthermore, the boson peak feature is seen even for the quenched normal

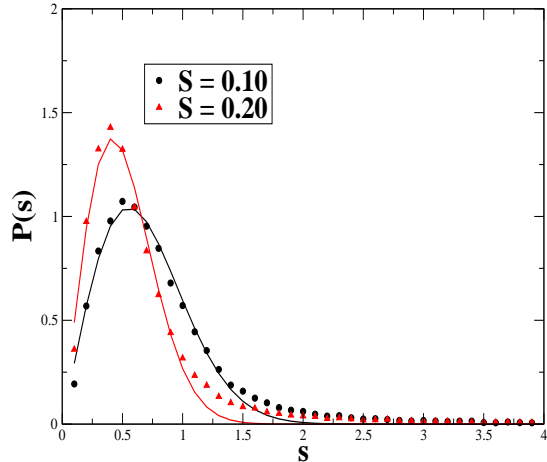


FIG. 11: The level spacing distribution,  $P(s)$  for  $S = 0.10$  and  $S = 0.20$  systems for the full eigen value spectrum. Data is shown for  $S = 0.10$  and  $S = 0.20$  systems at  $T = 0.50$ . The symbols are the data points and the thick lines are fit to the data according to the equation,  $P(s) = As^\beta \exp(-Bs^2)$ . The values of  $\beta$  are 1.02 and 1.08 for  $S = 0.10$  and  $S = 0.20$  systems, respectively.

modes obtained from equilibrium configurations at very high temperature (i.e.  $T \gg T_{MCT}$ ), as shown in FIGURE 10. As  $T$  increases, the boson peak height increases but the peak shifts to lower frequencies. Such a trend has been observed in experiments as well [29, 30]. However, the temperature-dependence is weak here. The boson peak feature at high temperatures shown in FIGURE 10 is to be contrasted with the observation made in an earlier paper[11] where the authors studied the appearance of the boson peak in soft sphere binary mixture. In their study, the authors found that as  $T$  increases above  $T_{MCT}$ , the boson peak feature disappears. The authors interpret the boson peak as a manifestation of an *underlying crossover of the parent liquid's configuration from a saddle dominated dynamics to a minima dominated behavior*. However, the observation of boson peak at high temperatures makes such an interpretation questionable.

The fragility of the current model polydisperse supercooled liquid decreases with polydispersity index,  $S$  [22]. This suggests an inverse correlation between the fragility of the liquid and the intensity of the boson peak. Such a correlation has actually been observed previously for many liquids in experiments [31] as well as in the simulation studies of model glass formers [13]. Shintani and Tanaka [13] carried out extensive simulations on 2D spin liquid glass former in which the fragility can be varied over an extremely wide range. This was achieved by varying the anisotropic part of the potential,  $\Delta$  which is a measure of the strength of frustration against crystallization. As already mentioned, the authors found an inverse correlation between the fragility and the intensity of the boson peak. In the current model system the

polydispersity index,  $S$  plays the same role as  $\Delta$ . Auer and Frenkel have shown that crystal nucleation in a polydisperse colloid is suppressed due to the increase of the surface free energy [32] and studies by several groups [33] show that the glassy amorphous phase becomes the equilibrium phase beyond a terminal value of polydispersity.

If a correlation between the fragility and the intensity of the boson peak exists, then it would mean that there is also a link between the fast intra-basin vibrational dynamics and the slow inter-basin diffusive dynamics (See [34]). However, it appears hard to reconcile such a *link* with the Adam-Gibbs paradigm as the latter predicts a relationship between the relaxation time,  $\tau$  and the configurational entropy,  $S_c$  ( $\tau \sim \exp(\frac{A}{TS_c})$ ). Clearly, on the time scale typical of vibrational dynamics (few pico seconds), the system would not have sampled sufficient configurations as would be necessary to define  $S_c$ . Hence it is difficult to understand the correlation between the intensity of the boson peak and fragility from this perspective.

It is interesting to note in this connection that Angell et al [35] have already suggested that the Boson peak can serve as a signature of configurational excitations of the ideal glass structure i.e. the topologically diverse defects of the glassy solid state. This means that the boson peak is related to the topographical features of the potential energy landscape and is thus involved in determining the fragility of the liquid. As already discussed in Section III A, at higher polydispersity we have *flatter* basins (FIGURE 8). This is consistent with the decrease in the fragility with  $S$ , as fragile liquids have rugged heterogeneous landscape whereas strong liquids have smoother landscapes, in accord with their constant activation energy predicted by their Arrhenius behavior [36].

The strong liquids in Angell's fragile/strong classification are usually network glass formers like  $SiO_2$ ,  $GeO_2$  etc., and they appear to lie almost on the opposite spectrum of our polydisperse liquid system. For a polydisperse LJ liquid, the decrease in fragility with polydispersity is via dynamic facilitation by smaller particles [22, 23]. An obvious manifestation of the dynamic facilitation is the size-dependent glass transition temperature [22]; as temperature is lowered the larger particles freeze in first, followed by the smaller ones. Therefore dynamic facilitation by polydispersity implies that at higher polydispersity not only the system has smaller barriers to diffusion but it also has more relaxation channels available to it.

Here it is interesting to note that Shirmacher et al [9] have shown that if a system of coupled harmonic oscillators (with spatially fluctuating nearest-neighbor force constants on a simple cubic lattice) is near the borderline of stability a low-frequency peak appears in  $g(\nu)/\nu^2$  as a precursor of the instability. In their model system, when the amount of the negative force constants becomes too large, the system becomes unstable and the boson peak feature shows up. Furthermore, as the fraction of negative force constants increases the peak intensity increases

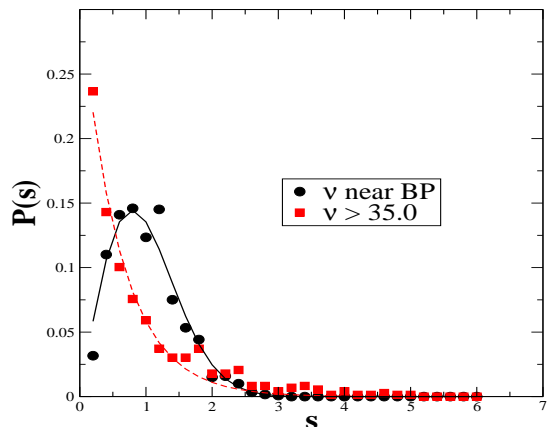


FIG. 12: The level spacing distribution,  $P(s)$  for the eigen values in the range  $3.0 \leq \nu \leq 4.0$  (near the boson peak) shown in circles and for eigen values in the high frequency range ( $\nu > 35.0$ ) shown by squares. Data is shown for  $S = 0.10$  at  $T = 0.50$ . The symbols are the data points and the thick lines are fit to the data according to the Gaussian orthogonal ensemble (thick line) and Poissonian distribution (dashed line)

and the peak shifts towards lower frequencies. Instantaneous normal mode analysis shows (see again FIGURE 4) that the fraction of unstable modes increases with polydispersity which implies more pathways for diffusion [16] at higher polydispersity. Thus the increase in the intensity of boson peak with polydispersity can be understood in terms of dynamic facilitation by polydispersity. The relationship with the strength/fragility of the system, however, still remains a bit unclear.

One of the key issues in the interpretation of the boson peak feature is whether the modes comprising it are localized or extended. Figure 7 shows that the modes at the frequency range where boson peak appears are largely delocalized with high values of participation ratio ( $PR > 0.6$ ). For frequencies less than  $\nu_{BP}$ , the participation ratio drops suddenly. This sudden drop of  $PR$  at low frequencies has been attributed to finite size effects [18]. These low-frequency modes have been shown to be extended, notwithstanding their low  $PR$  values. However, note that the frequency of the boson peak coincides with the frequency below which  $PR$  suddenly drops. The reason for this behavior is not clear to us. Furthermore, at the boson peak frequency, the  $PR$  decreases with  $S$  indicative of a correlation between localization of modes and boson peak intensity. These features are common to all the three system sizes ( $N=256, 500$  and  $864$ ) studied.

An alternate way to check whether the boson peak is indeed associated with localized modes (or not) is by means of level distance statistics [9, 37]. The level spacing distribution,  $P(s)$  for the random-matrix models is defined as the probability of finding the next-nearest-neighbor eigenvalue of the spectrum to be at a distance  $s$ , i.e.  $s = \frac{\nu_{i+1} - \nu_i}{D}$ , where  $D$  is the mean level spacing. In

the case of delocalized states, according to the Gaussian orthogonal random matrix ensemble, we get

$$P(s) = As^\beta \exp(-Bs^2) \quad (9)$$

For localized states, one gets a Poissonian distribution,  $P(s) = \exp(-s)$ . This is due to the fact that the delocalized states show level repulsion, whereas localized ones do not. In FIGURE 11 we have plotted the level spacing distribution  $P(s)$  for the full eigenvalue spectrum along with the fit for the orthogonal random matrix model. The values of  $\beta$  obtained from the fit are 1.02 and 1.08 for  $S = 0.10$  and  $S = 0.20$  systems, respectively. This shows that these systems display the behavior according to the Wigner surmise. In FIGURE 12, we plot the level spacing distribution for frequencies near the boson peak ( $3.0 \leq \nu \leq 4.0$ ) and also for the high frequencies ( $\nu > 35.0$ ) where the modes are truly localized (See 7). From the plot it is clear that statistics at high frequencies follow Poissonian distribution as expected for localized states. In the vicinity of the boson peak, however, we find a Gaussian distribution according to the Gaussian orthogonal random matrix ensemble, which means that the corresponding states are delocalized. However, it should be noted here that the transverse phonons are shown to be localized at the boson peak frequency according to the Ioffe-Regel criterion [9, 13].

#### IV. CONCLUDING REMARKS

Let us first summarize the main results of this paper. We have computed the vibrational density of states,  $g(\nu)$  in a polydisperse Lennard-Jones system, for three system sizes and three different polydispersity. Polydispersity is shown to have a significant effect on the vibrational density of states. Increase in the polydispersity leads to an increase in the localized high frequency modes. As polydispersity increases, there is a softening of vibrational modes manifested in the population shift from modes with frequencies above the maximum in  $g(\nu)$  to that below the maximum. The reduced density of states,  $g(\nu)/\nu^2$  exhibits the boson peak feature. The boson peak is seen to exist even for high temperature liquid configurations and shows a rather narrow sensitivity to temperature. The intensity of the boson peak increases with polydispersity, which can be understood in terms of dynamic facilitation by polydispersity by increase in fraction of the unstable modes.

The results clearly show a correlation between an increase in the peak height of the BP with an increase in the strength of the liquid – both are consequences of increase in polydispersity. This is in agreement with known experimental results. We find that while the modes comprising the BP are largely delocalized, there is a sharp drop in the PR of the modes that exist just below the BP. The last observation could be due to the finite size of the system. The delocalized nature of the BP appears

to be quite robust, within the three system sizes considered here, as supported both by the participation ratio and level spacing statistics.

The observed weak temperature dependence of the boson peak seem to suggest absence of any temperature mediated phase transition in the stationary points of the energy landscape from a saddle dominated to a minima dominated regime. However, all the evidences do suggest a close relation between boson peak and unstable modes of the system. The precise nature of these unsta-

ble modes, however, remains unclear at this point.

### Acknowledgments

We thank Professors Chandan Dasgupta and Srikanth Sastry for discussions. This work was supported in parts by grants from DST, India. S. E. Abraham acknowledges CSIR, India for a research fellowship.

- 
- [1] F. Sette et al, *Science* **280**, 1550 (1998).
  - [2] *Amorphous Solids- Low Temperature Properties*, edited by W. A. Philips, Topics in Current Physics Vol. 24 (Springer-Verlag, Berlin, 1981).
  - [3] T. Nakayama, *Physica B* **263-264**, 243 (1999).
  - [4] W. Shirmacher, *Europhys. Lett.* **73**, 892 (2006).
  - [5] A. I. Chumakov, I. Sergueev, U. van Brck, W. Schirmacher, T. Asthalter, R. Rffer, O. Leupold, and W. Petry, *Phys. Rev. Lett.* **92**, 245508 (2004).
  - [6] C. Oligschleger and H. R. Schober, *Phys. Rev. B* **59**, 811 (1999).
  - [7] Yu. G Vainer, A. V. Naumov, M. Bauer and L. Kaor, *Phys. Rev. Lett.* **97**, 185501 (2006).
  - [8] V. L. Gurevich, D. A. Parshin and H. R. Schober, *JETP Lett.* **76**, 553 (2002).
  - [9] W. Schirmacher, G. Diezemann and C. Ganter, *Phys. Rev. Lett.* **81**, 136 (1998).
  - [10] F. Leonforte, R. Boissiere, A. Tanguy, J. P. Wittmer and J. -L. Barrat, *Phys. Rev. B* **72**, 224206 (2005).
  - [11] T. S. Grigera, V. Martin-Mayor, G. Parisi and P. Verrocchio, *Nature* **422**, 289 (2003).
  - [12] V. Lubchenko and P. G. Wolynes, *Proc. Nat. Acad. Sci.* **100**, 1515 (2002).
  - [13] H. Shintai and H. Tanaka, *Nature Materials* **7**, 870 (2008).
  - [14] H. Cang, J. Li, H. C. Anderson and M. D. Fayer, *J. Chem. Phys.* **123**, 064508 (2005).
  - [15] S. R. Nagel, G. S. Grest and A. Rahman, *Phys. Rev. Lett.* **53**, 368 (1984).
  - [16] R. A. LaViolette and F. H. Stillinger, *J. Chem. Phys.* **83**, 4079 (1985).
  - [17] B. B. Laird and H. R. Schober, *Phys. Rev. Lett.* **66**, 636 (1991).
  - [18] V. Mazzacurati, G. Ruocco and M. Sampoli, *Euro. Phys. Lett.* **34**, 681 (1996).
  - [19] E. R. Weeks, J. C. Crocker, A. C. Levitt, A. Schofield, and D. A. Weitz, *Science* **287**, 627 (2000).
  - [20] S. C. Glotzer, V. N. Novikov and T. B. Schroder, *J. Chem. Phys.* **112**, 509 (2000).
  - [21] R. K. Murarka and B. Bagchi, *Phys. Rev. E* **67**, 051504 (2003).
  - [22] S. E. Abraham, S. M. Bhattacharyya and B. Bagchi, *Phys. Rev. Lett.* **100**, 167801 (2008).
  - [23] S. E. Abraham and B. Bagchi, *Phys. Rev. E* **78**, 051501 (2008).
  - [24] A. Rahman, M. J. Mandell and J. P. McTague, *J. Chem. Phys.* **64**, 1564 (1976).
  - [25] E. I. Takizawa and L. Kobayasi, *Chinese Jour. Phys.* **5**, 11 (1967).
  - [26] F. H. Stillinger and T. A. Weber, *Science* **225**, 983 (1984).
  - [27] F. H. Stillinger, *Science* **267**, 1939 (1995).
  - [28] S. Mossa, E. La Nave, H. E. Stanley, C. Donati, F. Sciortino and P. Tartaglia, *Phys. Rev. E* **65**, 041205 (2002).
  - [29] N. J. Tao, G. Li, X. Chen, W. M. Du and H. Z. Cummins, *Phys. Rev. A* **44**, 6665 (1991).
  - [30] D. Enberg, A. Wischniewski, U. Buchenau, L. Borjesson, A. Dianoux, A. P. Sokolov and L. M. Torell, *Phys. Rev. B* **59**, 4053 (1999).
  - [31] V. N. Novikov, Y. Ding and A. P. Sokolov, *Phys. Rev. E* **71**, 061501 (2005).
  - [32] S. Auer and D. Frenkel, *Nature* **413**, 711 (2001).
  - [33] P. Chaudhuri, Smarajit Karmakar, Chandan Dasgupta, H. R. Krishnamurthy and A. K. Sood, *Phys. Rev. Lett.* **95**, 248301 (2005); D. A. Kofke and P. G. Bolhuis, *Phys. Rev. E* **59**, 618 (1999); D. J. Lacks and J. R. Wienhoff, *J. Chem. Phys.* **111**, 398 (1999).
  - [34] T. Scopigno, G. Ruocco, F. Sette, G. Monaco, *Science* **302**, 849 (2003).
  - [35] C. A. Angell, Y. Yue, L. Wang, J. R. D. Copley, S. Borick and S. Mossa, *J. Phys: Condens. Matter* **15**, S1051 (2003).
  - [36] P. G. Debenedetti and F. H. Stillinger, *Nature* **410**, 259 (2001).
  - [37] F. M. Izrailev, *Phys. Rep.* **196**, 299 (1990).